Comparative Analysis of The Correction Effect of Different Environmental Loading Products On Global GNSS Coordinate Time Series

Yuefan He
GNSS Research Center
Guigen Nie (ggnie@whu.edu.cn)
Wuhan University https://orcid.org/0000-0003-1271-7968
Shuguang Wu
GNSS Research Center
Haiyang Li
GNSS Research Center

Full paper

Keywords: GNSS coordinate time series, Environmental loading products, RMS reduction rate, Amplitude, Phase

Posted Date: July 27th, 2021

DOI: https://doi.org/10.21203/rs.3.rs-724942/v1

Abstract

The global navigation satellite system (GNSS) coordinate time series is affected by the environmental loading (including atmospheric loading (ATML), hydrological loading (HYDL), non-tidal oceanic loading (NTOL), etc.) and many organizations now provide grid products of these loadings. The temporal and spatial resolutions of these products, the loading models and data sources used are not the same, so the effect of correcting the nonlinear deformation of the GNSS coordinate time series is obviously different. This study mainly selects the three agencies, namely, School and Observatory of Earth Sciences (EOST) in France, German Research Center for Geosciences (GFZ) in Germany, and International Mass Loading Service (IMLS) in the United States, including 6 types of ATML models, 7 types of HYDL models and 5 NTOL models. The classification of these 18 environmental loading models was discussed, and the root mean square (RMS) reduction rate of the GNSS coordinate time series after environmental loading corrections (ELCs) was used to evaluate the performance differences of various models. Our results show that both the different models provided by the same organization and the same model provided by different organizations have different correction effects. Regardless of the models, it has a significant impact on the vertical coordinate time series. In order to correct the nonlinear deformation of the GNSS stations to the greatest extent, based on the above analysis, this study selects the optimal model combination of three environmental loadings as ECMWF_IB+MERRA2+ECCO1, and then explores its influence on the periodic signals in the GNSS coordinate time series. Research suggests that environmental loadings have a significant impact on the amplitude and phase of GNSS time series. Especially in the vertical direction, the largest RMS value can reach 8.42 mm. Before and after ELCs, the maximal difference of the annual amplitude and the half-annual amplitude at global 631 stations can reach 8.96 mm and 1.51 mm, respectively. Among them, 84.60% of the stations were corrected by the optimal environmental loading combination model, thus the nonlinear deformation was weakened.

Introduction

In the past 20 years, many scholars have used GNSS coordinate time series to carry out different aspects of geoscience research work, mainly including periodic signal analysis in GNSS coordinate time series (Blewitt et al., 2001; Ray et al., 2008; Klos et al. al., 2018a, 2018b), stochastic model research (Williams et al., 2004; Langbein, 2008), environmental loading model (van Dam et al., 1994, 2001, 2010; Jiang et al., 2013a, 2014; Gu et al., 2017; Chanard et al., 2018; Yuan et al., 2018; Klos et al., 2018c) and other aspects. GNSS coordinate time series contains a lot of information about the elastic deformation of the earth caused by environmental factors such as the atmosphere, seabed pressure, snow, ice, surface water, and groundwater (Farrell, 1972; Li et al., 2020). Existing studies have shown that environmental loading factors including ATML, NTOL and HYDL are the main cause of nonlinear changes in GNSS time series (Jiang et al., 2010; Sun et al., 1995). By establishing the surface loading model and calculating the elastic deformation displacement sequence of GNSS stations, the geophysical influence mechanism at the station position can be effectively studied. At the same time, it compares and analyzes the characteristic changes of nonlinear deformation in the GNSS coordinate time series before and after the surface

loading correction, and detects the effects of various surface loadings on the GNSS coordinate time series. This is essential to correctly understand the geophysical sources of nonlinear changes in GNSS coordinate time series.

For ATML model, van Dam et al. (1994) analyzed the elevation time series of 19 global positioning system (GPS) stations in the northern hemisphere. They concluded that when the atmospheric loading correction was applied, the variance of the GPS elevation time series could be reduced by 24%, and the atmospheric loading displacement series fluctuates greatly in high latitude regions. van Dam et al. (2010) also found that when the influence of terrain factors on ATML was taken into account, the nonlinear motion of GPS elevation time series could be better explained. Li et al. (2020) calculated the surface displacement caused by five atmospheric loading products and compared them with the coordinate time series of 596 global GNSS stations. The results showed that the ERA-Interim model performed best in reducing the dispersion of GNSS coordinate time series, and for all five atmospheric models, the correction effect of inland stations was better than that of island stations.

For HYDL model, van Dam et al. (2001) analyzed the elevation time series of 147 GPS stations around the world. They found that HYDL can cause the RMS value of GPS elevation time series increase by 8 mm. After hydrological loading correction, the dispersion of the GPS height time series at 92 stations decreased. Dill and Dobslaw (2013) used a global high-resolution hydrological model. The study concluded that after corrections of ATML and NTOL, HYDL could explain up to about 54% of the vertical nonlinear deformation of GPS stations. Among these loadings, HYDL is an important factor that causes periodic vertical deformation of GPS stations (van Dam et al., 1998; Liao et al., 2010; Jiang et al., 2014). The increase of HYDL on land will cause the ground to sink, and the vertical position of GPS stations will move downward. The weakening of HYDL on land will cause surface to rebound, which will cause the vertical position of GPS stations to move upward.

For NTOL model, Williams and Penna (2011) studied the NTOL of 17 GPS stations at coastal areas of Europe. The study showed that the NTOL of these stations were of similar magnitude to ATML, and the sum of the two types of environmental loadings could explain about 20–30% of the RMS value of GPS elevation time series. On a global scale, the maximum NTOL calculated using the latest oceanic bottom pressure model could reduce the RMS value of GPS elevation time series by 3.7 mm. RMS values of about 70% global stations were reduced (van Dam et al., 2012).

For sum environmental loading (SUML) model, Dong et al. (2002) quantitatively calculated the impact of ATML, NTOL, HYDL and the sum of the three on 128 GPS stations around the world. The study indicated that SUML can explain about 40% of the seasonal signals in GPS elevation time series. Jiang et al. (2013b) studied the causes of nonlinear changes in 11 IGS stations in China, and believed that ELCs could effectively weaken the annual amplitude of GPS elevation time series, but the correction effect on horizontal component of GPS stations was not ideal. The displacement of the GNSS stations caused by the environmental loadings can reach several centimeters and produce a seasonal signal with an amplitude of millimeters, which not only has a significant impact on the estimated speed of these

stations (Johnson et al., 2017), but also deviates the establishment of the earth reference frame (Freymueller, 2009; Zou et al., 2014). By correcting environmental loadings, the nonlinear deformation in GPS coordinate time series can be reduced to a certain extent. Taking into account the differences of the surface loading data sources used by different agencies, the current surface loading models can explain up to 50% of the nonlinear deformation of GNSS stations in the ideal case, and less than 20% in the horizontal direction (Yan et al., 2009; Xu et al., 2017). Therefore, the ELCs cannot completely eliminate the nonlinear deformation in GNSS coordinate time series.

At present, many research institutions around the world provide environmental loading products, including GFZ (http://rz-vm115.gfz-potsdam.de:8080/repository) (Dill and Dobslaw., 2013), EOST (http://loading.u-strasbg.fr/) in Strasbourg, France (Mémin et al., 2020) and IMLS (http://massloading.net/#Download). In addition, softwares such as QOCA (Dong et al., 2002) and OMD (Jiang et al., 2013a) can also calculate the ground displacement caused by environmental loadings. Due to different measured data (such as global atmospheric pressure, ocean bottom pressure, land water reserves), different geophysical models and methods, the environmental loading displacement at the same stations obtained by the above institutions and softwares may be quite different. For example, Andrei et al. (2018) calculated the 15-year coordinate time series of the Finnish Antarctic research station, namely ABOA, and compared the environmental loading products provided by GFZ, EOST and IMLS. The study found that the non-tidal oceanic loadings given by GFZ and EOST were significantly different.

Therefore, this study selects 21-year coordinate time series of 631 International GNSS Service (IGS) reference stations around the world, and mainly compares 6 kinds of ATML products, 7 kinds of HYDL products and 5 kinds of NTOL products provided by EOST, GFZ and IMSL. We analyze the effects of various models on GNSS coordinate time series, then select the optimal three environmental loading models, and further explore their effects on periodic signals in GNSS coordinate time series.

Data And Model Description

2.1 GNSS coordinate time series

The GNSS coordinate time series data is acquired from Scripps Orbit and Permanent Array Center (SOPAC), a data analysis center organized by IGS. This organization provides not only raw data with outliers and offsets in GNSS coordinate time series, but also clean data removing outliers. In this study, we mainly use the detrended mean GNSS time series (CleanDetrend) after removing offsets (caused by coseismic or noncoseismic reasons) and outliers, and retain the seasonal period term. The data is downloaded from ftp://garner.ucsd .edu/archive/garner/timeseries/measures/ats/.

Before data analysis, this study needs to select the acquired data from 2000 to 2021. The selection criteria are as follows. First, within recent past 21 years, the length of GNSS time series shall not be less than 3 years to ensure data integrity and the reliability of following processing results. Then, delete sites with obvious abnormal non-linear motions, including obvious post seismic deformations, local surface

deformations, or abnormal motions caused by other unknown causes. Through the elimination of the above steps, 631 sites around the world are finally selected for data processing. The distribution of GNSS stations is shown in Fig. 1.

2.2 ATML model

The ATML model used in this paper includes 6 kinds of loading displacement data relative to the Earth's center of figure, among which three are provided by EOST. The first ECMWF_IB model estimated from European Centre for Medium Range Weather Forecasts (ECMWF) operational model, assuming an inverted barometer ocean response to pressure forcing. The second is the ECMWF model, which estimated from surface pressure from ECMWF operational model, assuming a dynamic ocean response to pressure & winds from TUGO-m barotropic model (Carrère and Lyard., 2003). The third type is the era interim (ERA-interim) model. It is estimated from surface pressure from ERA interim (ECMWF Reanalysis) model, assuming an inverted barometer ocean response to pressure forcing. In addition, there is the ECMWF model provided by GFZ. The data is the elastic surface loading deformation value calculated by the method of repairing the Green function. The other two models are the Global Earth Observing System Forward Processing Instrumental Team (GEOSFPIT) model and the Modern-Era Retrospective analysis for Research and Applications, version 2 (MERRA2) model provided by IMLS of the National Aeronautics and Space Administration (NASA). The spatial, time resolution and time span of the six ATML models provided by the above three agencies are shown in Table 1.

Table 1
Six commonly-used ATML from EOST, GFZ and IMSL

Type	Institution	Model	Spatial Resolution	Time Resolution	Time Span
ATML	EOST	ECMWF(IB)	0.5°× 0.5°	3h	2000-present
		ECMWF	0.5°× 0.5°	3h	2002–2017
		ERA interim	0.5°× 0.5°	6h	1979-present
	GFZ	ECMWF	0.5°× 0.5°	3h	1976-present
	IMSL	GEOSFPIT	2′ × 2′	3h	2000-present
		MERRA2	2′ × 2′	6h	1980-present

2.3 HYDL model

The HYDL models used in this paper includes 7 types, which also come from EOST, GFZ and IMSL. Among them, HYDL models provided by EOST include Global Land Data Assimilation System, Phase (GLDAS1) and GLDAS2. The HYDL includes soil moisture, snow and canopy water, estimated according to the GLDAS/Noah v1.0 model, and areas covered by permanent snow and ice (Greenland, Alaska, Alpine glaciers, etc.) have been obscured (Rodell et al., 2004). In MERRA2 model, only soil moisture and snow are considered. Similarly, areas covered by permanent ice and snow have been masked (Gelaro et al., 2017). For the MERRA-land model, the HYDL includes soil moisture and snow. According to the

MERRA-land model, the area covered by permanent ice and snow has also been masked (Reichle et al., 2011). The hydrological loading data model calculated by GFZ is the Land Surface Discharge Model (LSDM, Dill, 2008). The physics and parameterization of LSDM is based on the research of Hagemann and Dümenil (1998). LSDM includes soil moisture, shallow groundwater, snow cover, and surface water stored in rivers and lakes (Hagemann and Dümenil,1998). The last two HYDL models are the Global Earth Observing System Forward Processing Instrumental Team (GEOSFPIT) and MERRA2 models provided by IMLS. The time and spatial resolution and time span of the seven HYDL models used are shown in Table 2.

Table 2
Seven commonly-used HYDL from EOST, GFZ and IMSL

Type	Institution	Model	Spatial Resolution	Time Resolution	Time Span
HYDL	EOST	GLDAS1	0.5°× 0.5°	3h	2000–2016
		GLDAS2	0.5°× 0.5°	3h	1980-present
		MERRA2	0.5°× 0.625°	1h	1980–2019
		MERRA-land	0.5°× 0.67°	1h	1980–2016
	GFZ	LSDM	0.5°× 0.5°	24h	1976-present
	IMSL	GEOSFPIT	2′ × 2′	3h	2000-present
		MERRA2	2′ × 2′	3h	1980-present

2.4 NTOL model

This paper uses five NTOL models, including Estimating the Circulation and Climate of the Ocean (ECCO1) model provided by EOST, which is the non-tidal oceanic loading estimated based on ECCO1 (kf080i) seabed pressure. ECCO2 (follow-on ECCO, Phase II) model is a NTOL estimated based on the ECCO2 seabed pressure (Menemenlis et al., 2008). The GLobal Ocean ReanalYses and Simulations (GLORYS2v3) model is a non-tidal oceanic loading model estimated based on the GLORYS2v3 seabed pressure. The Max Planck Institute Ocean Model (EMPIOM) model provided by GFZ using the same ECMWF operating data and the MPIOM06 model provided by IMSL. The temporal and spatial resolutions and time span of these five NTOL models are shown in Table 3.

Table 3
Five commonly-used NTOL from EOST, GFZ and IMSL

Type	Institution	Model	Spatial Resolution	Time Resulotion	Time Span
NTOL	EOST	ECCO1	1°× 1°	12h	1993-present
		ECCO2	0.5°× 0.5°	24h	1992-present
		GLORYS2v3	0.5°× 0.5°	24h	1992–2013
	GFZ	EMPIOM	1°× 1°	3h	1976-present
	IMSL	MPIOM06	2′ × 2′	3h	1980-present

Methodology

GNSS coordinate time series can be divided into two parts, namely, deterministic model and stochastic model (Bevis and Brown., 2014). The former is composed of linear trend, periodical terms (including annual, and half annual signals, etc.) and offsets. The latter mainly refers to noise. GNSS coordinate time series is represented by the following function model.

$$y(t_i) = y_0 + vt_i + \sum_{k=1}^{q} a_k \sin(2\pi f_k t_i) + b_k \cos(2\pi f_k t_i) + \sum_{j=1}^{n_g} g_j H(t_i - T_{gj}) + r(t_i) \quad (1)$$

Among them, y_0 represents the intercept; v is the linear velocity in a year, where a year is defined as 365.25 days; t_i is the epoch of GNSS time series; a_k, b_k represents the amplitude of the periodic signal; f_k refers to the corresponding frequency; g_i and T_{gi} are the offset and the corresponding epoch respectively; r is the residual time series. H represents the Heaviside step function, which is expressed as follows:

$$\begin{cases} H(t) = 0, t < 0 \\ H(t) = 0.5, t = 0 \\ H(t) = 1, t > 0 \end{cases} \quad (2)$$

In this article, we use correlation coefficients and RMS reduction rates to evaluate the correction effects of different environmental loading products. Before calculating these indicators, we need to deduct the linear trend term from the GNSS time series. The RMS reduction rate is expressed as follows:

$$RMS_{reduction}(\%) = \frac{RMS_{original} - RMS_{corrected}}{RMS_{original}} \times 100\% \quad (3)$$

Among them, $RMS_{original}$ and $RMS_{corrected}$ respectively represent RMS value of the GNSS coordinate time series before and after ELCs, and RMS reduction rate can be used as an index to measure the contribution of the loading models to GNSS coordinate time series. The larger of $RMS_{reduction}$ value, the better of the correction effect of environmental loading models.

This paper also introduces amplitude and phase of annual and half-annual signals to quantitatively evaluate the contribution of environmental loading effects to nonlinear changes of GNSS coordinate time series. The difference of annual/half-annual amplitude and phase before and after ELCs is as follows.

$A_{difference} = A_{original} - A_{corrected}$ (4)

Among them, $A_{original}$, $A_{corrected}$ represents the annual amplitude or phase before and after ELCs, and the half-annual amplitude or half-annual phase. When $A_{difference}$ is a positive value, it indicates that the non-linear change amplitude of GNSS coordinate time series is weakened after ELCs.

Conclusion And Analysis

4.1 Comparison of products with different environmental loadings

4.1.1 ATML products

First, obtain the coordinate time series of 631 GNSS stations around the world from 2000 to 2021, and then use the six ATML models mentioned above, including ECMWF_IB, ECMWF, and ERA interim provided by EOST, ECMWF provided by GFZ, GEOSFPIT and MERRA2 provided by IMSL. RMS reduction rate of GNSS coordinate time series before and after the ATML correction is used to compare and analyze the correction effects of the six ATML models.

As shown in Fig. 2 to Fig. 4, this paper calculates RMS reduction rate of three-dimensional coordinate components of GNSS stations after the correction of six ATML models. Figure 2 shows the distribution of RMS reduction rates after six ATML corrections, and the percentage of GPS stations whose reduction rate is positive is marked at the upper right of each panel. It can be seen from Fig. 2 that in N direction, the model with the largest percentage of positive reduction rate (64.98%) is ECMWF_IB provided by EOST. The model with the smallest percentage of positive reduction rate (50.40%) is GEOSFPIT provided by IMSL. It can be seen from Fig. 3 that in E direction, the model with the largest percentage of positive reduction rate (66.40%) is still the ECMWF_IB model provided by EOST. The model with the smallest reduction rate is still GEOSFPIT model provided by IMSL, with a ratio of 52.14%. It can be seen from Fig. 4 that in U direction, the model with the largest percentage of positive reduction rate (80.98%) is ECMWF

model provided by EOST. The reduction rate with the smallest positive value is GEOSFPIT model provided by IMSL, with a ratio of up to 60.70%.

At the same time, this article also counts the maximum reduction rate of each model in N, E and U directions, as shown in Table 4. The maximum reduction rate in each direction is the ECMWF model provided by EOST, which can reach 81.68%, 75.26% and 82.57% respectively. It indicates that the ATML model, ECMWF from EOST, has played a very active role in some GNSS stations. From Fig. 2 to Fig. 4, we can also see that even if the same ATML model provided by different agencies, the RMS reduction rate is not exactly the same. For example, the ECMWF model provided by EOST has a ratio of 60.22%, 61.97%, and 80.98% in the three directions of N, E, and U, respectively. However, the ECMWF model provided by GFZ has a positive RMS reduction rate of 51.03%, 63.07%, and 77.97% in these three directions. This may be related to the method of model establishment. The ATML model provided by EOST is estimated by the surface pressure of the ECMWF operating model, and the GFZ data is the elastic surface loading deformation value calculated by the method of repairing the Green's function. In addition, comparing Fig. 4 with Fig. 2 and Fig. 3, it can be seen that in the vertical component, the RMS reduction rate of the six ATML models is generally higher than that of the horizontal component. This shows that no matter what kind of ATML model, the influence on the vertical direction is significantly greater than that on the horizontal direction.

Table 4
Statistical table of the maximum RMS reduction rate after 6 ATML corrections (%)

ATML models	N	E	U
EOST-ECMWF_IB	49.75	54.32	49.40
EOST-ECMWF	81.68	75.26	82.57
EOST-ERA interim	47.52	54.43	49.29
GFZ-ECMWF	47.61	41.65	49.25
IMSL-GEOSFPIT	47.36	40.26	47.75
IMSL-MERRA2	43.36	40.57	61.27

4.1.2 HYDL products

Consistent with the ATML comparison method, this section still uses RMS reduction rate to analyze the impact of the seven HYDL models GLDAS1, GLDAS2, MERRA2, MERRA-land, LSDM, GEOSFPIT and MERRA2 (IMSL) on GNSS coordinate time series provided by EOST, GFZ and IMSL. It can be seen from Fig. 5 that in N direction, the model with the largest percentage of positive reduction rate (60.70%) is MERRA-land provided by EOST, and the smallest percentage of positive reduction rate (45.64) is LSDM provided by GFZ. It can be seen from Fig. 6 that in E direction, the model with the largest percentage of positive reduction rate (61.97%) is MERRA2 provided by EOST, and the smallest percentage of positive reduction rate (46.43%) is still LSDM model provided by GFZ. It can be seen from Fig. 7 that in U direction,

the model with the largest percentage of positive reduction rate (81.93%) is MERRA2 provided by EOST, and the smallest percentage of positive reduction rate (60.06) is still LSDM provided by GFZ. In general, after comparing these seven hydrological loading models, it is found that the relatively optimal performance is the MERRA2 model provided by EOST.

At the same time, in the vertical component, all HYDL models have more significant effects than the horizontal component. After more than half of the stations have been corrected by the HYDL products in U direction, their RMS reduction rates have been significantly improved. Of course, similar to the atmospheric loading model, the same model provided by different agencies reflects different model performances when analyzing GNSS coordinate time series of 631 stations around the world. For example, in MERRA2 model provided by EOST and IMSL, the percentages of positive RMS reduction rate of each component are inconsistent. In N direction, the percentage of MERRA2 model provided by EOST is 57.53%, and the MARRA2 model provided by IMSL is 51.19%. The E direction is 61.97% and 55.94%, and the U direction is 81.93% and 68.62%, respectively. Therefore, when discussing the influence of HYDL model on GNSS coordinate time series in the future, even if it is the same loading model, the name of the source organization must be clearly marked. Finally, this section still counts the maximum reduction rate of each direction of HYDL model. It can be seen from Table 5 that GLDAS1 model provided by EOST has the largest reduction rate in N and E directions, which are 79.28% and 75.84% respectively. The maximum value in U direction is GLDAS2 model provided by EOST, which is 81.69%. This still shows that GLDAS has played a very active role in some stations.

Table 5
Statistical table of the maximum RMS reduction rate after 7 HYDL corrections (%)

HYDL models	N	E	U
EOST-GLDAS1	79.28	75.84	81.01
EOST-GLDAS2	79.04	75.36	81.69
EOST-MERRA2	46.91	56.25	54.56
EOST-MERRA-land	76.81	74.55	79.55
GFZ-LSDM	45.14	40.43	53.26
IMSL-GEOSFPIT	40.52	40.69	38.68
IMSL-MERRA2	44.65	40.88	54.48

4.1.3 NTOL products

This section still uses RMS reduction rate before and after loading correction to compare the effect of NTOL on GNSS time series. The selected NTOL models include ECCO1, ECCO2 and GLORYS2v3 provided by EOST, EMPIOM provided by GFZ and MPIOM06 provided by IMSL.

It can be seen from Fig. 8 to Fig. 10 that the RMS reduction rate of the NTOL is different in different dimensions. In general, the reduction rate in the vertical component is greater than the horizontal component. Moreover, the five NTOL models corresponding to the respective components have different percentage of positive reduction rates. As shown in Fig. 8, in N direction, the model with the largest percentage of positive reduction rate (62.60%) is ECCO1 provided by EOST, and the smallest percentage of positive reduction rate (49.29%) is EMPIOM provided by GFZ. It can be seen from Fig. 9 that in E direction, the model with the largest percentage of positive reduction rate (64.18%) is still ECCO1 provided by EOST, and the smallest percentage of positive reduction rate (50.24%) is still EMPIOM model provided by GFZ. From Fig. 10, in U direction, the model with the largest percentage of positive reduction rate (80.35%) is EMPIOM provided by GFZ, and the smallest percentage of positive reduction rate (61.97%) is GLORYS2v3 provided by EOST. For some NTOL models, the impact on the horizontal component may be small, but when compared on the vertical component, the impact is more significant, such as EMPIOM model provided by GFZ. Therefore, when analyzing the impact of non-tidal oceanic loading on GNSS coordinate time series, the components must be discussed separately.

Finally, this article counts the maximum value of the RMS reduction rate, as shown in Table 6. The maximum RMS reduction rate of NTOL in N, E and U directions are all GLORYS2v3 models provided by EOST. The values are 84.52%, 83.64% and 82.44%, respectively. This can also show that the NTOL model GLORYS2v3 has played a very good role in some stations.

Table 6
Statistical table of the maximum RMS reduction rate after 5 NTOL corrections (%)

NTOL models	N	E	U
EOST-ECCO1	45.66	41.38	51.21
EOST-ECCO2	46.71	41.41	50.41
EOST-GLORYS2v3	84.52	83.64	82.44
GFZ-EMPIOM	44.36	41.32	50.22
IMSL-MPIOM06	44.64	41.12	49.37

4.2 The optimal combination of environmental loading models

In this paper, statistics are made on 6 atmospheric loading models, 7 hydrological loading models and 5 non-tidal oceanic loading models provided by EOST, GFZ and IMSL. The percentage of GNSS stations with positive RMS reduction rates before and after the correction of these loading models are calculated, and the results are discussed and explained above one by one. In this section, the positive RMS reduction rates of above 18 models in N, E and U directions are averaged. Then compare these averages to find the optimal combination of environmental loading models on a global scale. The result is shown in Fig. 11.

It can be seen from Fig. 11 that among the six ATML models, the positive RMS reduction rate with the largest average percentage is ECMWF_IB provided by EOST. As indicated by the purple histogram in Fig. 11(a), the percentage can reach 69.41%. Therefore, this article selects ECMWF_IB as the optimal ATML model. At the same time, among the seven HYDL models, the MERRA2 provided by EOST has the largest average percentage of positive RMS reduction rate, which is represented by the brown histogram in Fig. 11(b), and the percentage can reach 67.14%. Therefore, the MERRA2 provided by EOST is selected as the optimal HYDL model. By analogy, the optimal model among the five NTOL models is the ECCO1 provided by EOST, which is represented by the red histogram in Fig. 11(c). The average percentage of positive RMS reduction rate can reach 67.67%. This article next focuses on the combination of these three optimal environmental loading models as ECMWF_IB + MERRA2 + ECCO1 to analyze their impact on nonlinear changes in GNSS coordinate time series.

4.3 The influence of the optimal ELCs on GNSS coordinate time series

The optimal atmospheric loading model ECMWF_IB, hydrological loading model MERRA2 and non-tidal oceanic loading model ECCO1 provided by EOST are used as the optimal environmental loading model combination to be discussed. In this study, the displacement sequences of these three environmental load models are cumulatively summed to further explore the nonlinear impact of the ELCs on global GNSS coordinate time series. First of all, this study analyzes and explains the magnitude of its impact. As shown in Fig. 12, in N direction, the maximum RMS value is 1.13 mm, in E direction, the maximum RMS value is 1.25 mm, and in U direction, the maximum RMS value can reach 8.42 mm. And from the RMS distribution diagrams in the three directions, it can be seen that the magnitude of the environmental loading impact in horizontal direction is still smaller than vertical direction. This shows that the environmental loading has a greater impact on GNSS coordinate time series in vertical direction, and it can be seen from Fig. 12 that the impact value is significantly greater in the middle and high latitude regions than in the low latitude regions.

From above analysis, it can be seen that the environmental loading has a non-negligible impact on the nonlinear deformation of GNSS coordinate time series, so this study uses Hector software to obtain the annual and half-annual amplitude and phase of GNSS coordinate time series (Bos et al., 2013, 2016). Discuss the influence magnitude of annual and half-annual amplitude and phase before and after the ELCs. The result is shown in Fig. 13.

When only white noise + flicker noise is considered, the GNSS coordinate time series have obvious annual amplitude and phase changes before and after ELCs. In E direction, the maximum annual amplitude difference can reach 1.68 mm. In 98.57% of the stations, the absolute values of the annual amplitude differences are less than 1 mm. In N direction, the maximum annual amplitude difference is 1.69 mm. In 98.09% of the stations, the absolute values of the annual amplitude differences are less than 1 mm. In U direction, the maximum annual amplitude difference can reach 8.96 mm, and 97.94% of the stations have an absolute value of the annual amplitude difference between 0 and 6 mm, and the magnitude of

the impact is significantly greater than in the horizontal direction. At the same time, in E, N and U directions, 46.19%, 43.02% and 84.60% of the stations were corrected for environmental loading, and their non-linear amplitude was weakened. It can be further seen that non-linear influence of environmental loading on GNSS coordinate time series is mainly reflected in the vertical direction.

In addition to annual amplitude difference, this article also statistically explains annual phase difference, as shown in Fig. 14. In E, N and U directions, the maximum absolute value of annual phase difference before and after ELCs are 178.55°, 179.15° and 174.62°, respectively. More than half of the stations have absolute annual phase differences between 0° and 60°, accounting for 80.47%, 73.01% and 72.22%, respectively. Compared with the influence of annual amplitude, the ELCs on the annual phase is not significantly different in the vertical and horizontal directions, but the magnitude is more obvious in the three directions. Therefore, when considering the impact of environmental loading on annual phase, the three directions of N, E and U need to be taken into consideration.

In addition to annual amplitude and phase, the environmental loading also has a more obvious impact on half-annual amplitude and half-annual phase of GNSS coordinate time series. As shown in Fig. 15, compared with the half-annual amplitude change in horizontal direction, the environmental loading has a more obvious influence in vertical direction, and the maximum difference can reach 1.51 mm. The maximum value of the half-annual amplitude difference in horizontal direction is less than 1 mm. Compared with the influence of annual amplitude, the impact of environmental loading on half-annual amplitude is smaller. When considering the impact of environmental loading on half-annual amplitude, the vertical direction is the top priority. In addition to half-annual amplitude, this study also provides a statistical description of half-annual phase difference, as shown in Fig. 16. In the three directions of E, N and U, the maximum values of half-annual phase differences are 179.68°, 179.73° and 178.39°, respectively. There are 89.21%, 81.90% and 85.71% of the stations, and the absolute value of half-annual phase difference is less than 60°. Therefore, compared with annual phase, the ratio is larger, which can show that the impact on annual phase is greater than half-annual phase before and after ELCs.

Summary

This study selects 631 GNSS coordinate time series that span from 2000 to 2021 globally. A total of 18 environmental loading products, including 6 atmospheric loading, 7 hydrological loading and 5 non-tidal oceanic loading provided by EOST, GFZ and IMLS, were compared and analyzed. Among them, for the five ATML products, in three directions of N, E and U, the maximum average percentage of positive RMS reduction is ECMWF_IB provided by EOST, and its rate can reach 69.41%. For the seven HYDL products, the maximum average percentage of positive RMS reduction is MERRA2 provided by EOST, and its ratio can reach 67.14%. For the five NTOL products, the maximum average percentage of positive RMS reduction is ECCO1 provided by EOST, and the rate can reach 67.67%. Therefore, these three environmental loading models ECMWF_IB + MERRA2 + ECCO1 are selected as the optimal model for cumulative analysis to obtain their influence on the nonlinear factors of GNSS coordinate time series.

Using the RMS reduction rate to classify and analyze the 18 environmental loading models, the results show that whether it is an ATML product, a HYDL product or a NTOL product, the influence on the vertical component is more significant than that of the horizontal component. For ATML models ECMWF_IB, ECMWF, ERA interim, ECMWF (GFZ), GEOSFPIT and MERRA2, the percentage of positive RMS reduction rate on vertical component can reach 76.86%, 80.98%, 76.23%, 77.97%, 60.70% and 68.94%, respectively. For HYDL models GLDAS1, GLDAS2, MERRA2, MERRA-land, LSDM, GEOSFPIT and MERRA2 (IMLS), the percentage of positive RMS reduction rate on vertical component can reach 74.80%, 74.64%, 81.93%, 77.65%, 60.06%, 63.71% and 68.62%, respectively. For NTOL models ECCO1, ECCO2, GLORYS2v3, EMPIOM and MPIOM06, the percentage of positive RMS reduction rate can reach 76.23%, 67.35%, 61.97%, 80.35% and 66.40%, respectively. It can be seen that in terms of the vertical component, more than half of the IGS stations of all loading models have played an active role. And the same model provided by different agencies and the different loading models provided by same agency play different roles. Therefore, in the later discussion and analysis, the data source and model name must be indicated.

Using the optimal environmental loading model combination obtained from the above analysis, the cumulative effect of ELCs on the periodic factors in GNSS coordinate time series is obtained. The results show that annual amplitude and half-annual amplitude mainly have a non-negligible effect on vertical direction. The annual amplitude difference and half-annual amplitude difference can reach 8.96 mm and 1.51 mm, respectively. After the ELCs, 84.60% of the non-linear deformation of the stations have been corrected. In horizontal direction, the impact is small, both less than 2mm. As for the results of annual phase and half-annual phase, it can be seen that whether it is horizontal component or vertical component, the environmental loading will have a non-negligible impact on it. Especially for annual phase, there are 19.67%, 26.98% and 27.95% of the stations in E, N and U directions, and the absolute value of phase differences are greater than 60°. Therefore, when studying the influence of environmental loading on the phase in GNSS coordinate time series, the horizontal and vertical component need to be discussed separately.

Abbreviations

GNSS: Global navigation satellite system; EOST: School and Observatory of Earth Sciences; GFZ: German Research Center for Geosciences; IMLS: International Mass Loading Service; ECMWF: European Centre for Medium-Range Weather Forecasts; ERA-interim: Era-interim; GEOSFPIT: Global Earth Observing System Forward Processing Instrumental Team; MERRA2: Modern-Era Retrospective analysis for Research and Applications, version 2; GLDAS: Global Land Data Assimilation System; LSDM: Land Surface Discharge Model; GEOSFPIT: Global Earth Observing System Forward Processing Instrumental Team; ECCO1: Estimating the Circulation and Climate of the Ocean; ECCO2: Follow-on ECCO, Phase □; GLORYS: GLobal Ocean ReanalYses and Simulations; MPIOM: Max Planck Institute Ocean Model; EMPIOM: 3 hourly ocean model MPIOM; MPIOM06: 6 hourly ocean model MPIOM; ELCs: Environmental loading corrections; RMS: Root mean square; ATML: Atmospheric loading; NTOL: Non-tidal oceanic loading; HYDL: Hydrological loading; GPS: Global positioning system; SUML: Sum environmental loading;

SOPAC: Scripps Orbit and Permanent Array Center; IGS: International GNSS Service; NASA: National Aeronautics and Space Administration.

Declarations

Availability of data and materials

The GNSS coordinate time series date, ATML data, HYDL data, NTOL data used in this study can be accessed at ftp://garner.ucsd .edu/archive/garner/timeseries/measures/ats/, http://rz-vm115.gfz-potsdam.de:8080/repository, http://loading.u-strasbg.fr/ and http://massloading.net/#Download, respectively.

Competing interests

The authors declare that they have no competing interests.

Funding

This research was funded by the National Natural Science Foundation of China (Grant No.41074023) and the National key Research and Development Scheme Strategic International Coopearation in Science and Technology Innovtion Program (No.2018YFE0206500).

Authors' contributions

YH: conceptualization, methodology, data processing, writing and editing. GN: supervision and original draft preparation. SW: data validation and editing. HL: resources and formal analysis. All authors read and approved the final manuscript.

Acknowledgements

We acknowledge the German Geoscience Research Center (GFZ), School and Observatory of Earth Sciences (EOST) in Strasbourg, France and International Mass Load Service (IMLS) who provided environmental loading products. The 631 GNSS coordinate time series in this article were provided by SOPAC. The Hector software (http://segal.ubi.pt/hector/) was used to calculate and analyze GNSS coordinate time series. We used GMT and Origin software to plot the calculation results. We express our heartfelt thanks to these organizations and software providers.

References

1. Andrei C, Lahtinen S, Nordman M, Näränen J, Koivula H, Poutanen M, Hyyppä J (2018) GPS time series analysis from ABOA the finnish antarctic research station. Remote Sensing 10(12)
2. Blewitt G, Lavallee D, Clarke P, Nurutdinov K (2001) A new global mode of Earth deformation: Seasonal cycle detected. Science 294:2342–2345. https://doi.org/10.1126/science.1065328

3. Bos MS, Fernandes RMS, Williams SDP et al (2013) Fast error analysis of continuous GNSS observations with missing data. J Geodesy 87(4):351–360. https://doi.org/10.1007/s00190-012-0605-0
4. Bos MS, Fernandes RM S (2016) Hector user manual version 1.6. http://segal.ubi.pt/hector/manual_1.6.pdf
5. Bevis M, Brown A (2014) Trajectory models and reference frames for crustal motion geodesy. J Geodesy 88:283–311. https://doi.org/10.1007/s00190-013-0685-5
6. Carrère L, Lyard F (2003) Modeling the barotropic response of the global ocean to atmospheric wind and pressure forcing comparisons with observations. Geophys Res Lett 30(6). https://doi.org/10.1029/2002GL016473
7. Chanard K, Fleitout L, Calais E, Rebischung P, Avouac J (2018) Toward a global horizontal and vertical elastic load deforma-tion model derived from GRACE and GNSS station position time series. Journal of Geophysical Research Solid Earth 123:3225–3237. https://doi.org/10.1002/2017JB015245
8. Dill R, Dobslaw H (2013) Numerical simulations of global scale high-resolution hydrological crustal deformations. Journal of Geophysical Research Solid Earth 118:5008–5017. https://doi.org/10.1002/jgrb.50353
9. Dill R (2008) Hydrological model LSDM for operational Earth rotation and gravity field variations. GFZ. https://doi.org/11.2312/GFZ.b103-08095
10. Dong D, Fang P, Bock Y, Cheng MK, Miyazaki S (2002) Anatomy of apparent seasonal variations from GPS-derived site position time series. Journal of Geophysical Research Solid Earth 107: ETG 9 – 1–ETG 9–16. https://doi.org/10.1029/2001JB000573
11. Farrell WE (1972) Deformation of the earth by surface loads. Rev Geophys 10(3):761–797. https://doi.org/10.1029/RG010i003p00761
12. Freymueller J (2009) Seasonal position variations and regional reference frame realization. In: Bosch W, Drewes H (eds) GRF2006 symposium proceedings. International Association of Geodesy symposia, 134:191–196. https://doi.org/10.1007/978-3-642-00860-3_30
13. Gu Y, Yuan L, Fan D, You W, Su Y (2017) Seasonal crustal vertical deformation induced by environmental mass loading in mainland China derived from GPS, GRACE and surface loading models. Adv Space Res 59:88–102. https://doi.org/10.1016/j.asr.2016.09.008
14. Gelaro R, McCarty W, Suárez MJ et al (2017) The Modern-Era Retrospective Analysis for Research and Applications, Version 2 (MERRA-2). J Clim 30:5419–5454
15. Hagemann S, Dümenil L (1998) A parametrization of the lateral waterflow for the global scale. Clim Dyn 14(1):17–31. https://doi.org/10.1007/s003820050205. 37
16. Jiang W, Li Z, van Dam T, Ding W (2013a) Comparative Analysis of Different Environmental Loading Methods and Their Impacts on the GPS Height Time Series. J Geodesy 87(7):687–703. https://doi.org/10.1007/s00190-013-0642-3

17. Jiang W, Li Z, Liu H et al (2013b) Cause analysis of the non-linear variation of the IGS reference station coordinate time series inside China. Chinese Journal of Geophysics 56(007):2228–2237
18. Jiang W, Xia C, Li Z et al (2014) Analysis of environmental loading effects on regional GPS coordinate time series. Acta Geodaetica Cartogr Sin 43(12):1217–1223. https://doi.org/10.13485/j.cnki.11-2089.2014.0149
19. Johnson CW, Fu Y, R Bürgmann (2017) Stress Models of the Annual Hydrospheric, Atmospheric, Thermal, and Tidal Loading Cycles on California Faults: Perturbation of Background Stress and Changes in Seismicity. Journal of Geophysical Research Solid Earth 122(12):10605–10625. https://doi.org/10.1002/2017JB014778
20. Jiang Zhihao Z, Peng M, Jinzhong L Lifen (2010) Velocity Estimation on the Colored Noise Properties of CORS Network in China Based on the CGCS2000 Frame. Acta Geodaetica et Cartographica Sinica (in Chinese). 39(4): 355–363
21. Klos A, Bos MS, Bogusz J (2018a) Detecting time-varying seasonal signal in gps position time series with different noise levels. GPS Solutions 22(1):21. https://doi.org/10.1007/s10291-017-0686-6
22. Klos A, Olivares G, Teferle FN, Hunegnaw A, Bogusz J (2018b) On the combined effect of periodic signals and colored noise on velocity uncertainties. GPS Solutions 22(1):1–13. https://doi.org/10.1007/s10291-017-0674-x
23. Klos A, Gruszczynska M, Bos M, Boy J, Bogusz J (2018c) Estimates of vertical velocity errors for IGS ITRF2014 stations by applying the improved singular spectrum analysis method and environmental loading models. Pure appl Geophys 175(5):1823–1840. https://doi.org/10.1007/s00024-017-1494-1
24. Li C, Huang S, Chen Q et al (2020) Quantitative Evaluation of Environmental Loading Induced Displacement Products for Correcting GNSS Time Series in CMONOC. Remote sensing 12(4):594. https://doi.org/10.3390/rs12040594
25. Li Z, Chen W, van Dam T, Rebischung P, Altamimi Z (2020) Comparative analysis of different atmospheric surface pressure models and their impacts on daily ITRF2014 GNSS residual time series. J Geodesy 94:42–61. https://doi.org/10.1007/s00190-020-01370-y
26. Liao HH, Zhong M, Zhou XH (2010) Climate driven annual vertical deformation of the solid earth calculated from GRACE. Chinese Journal of Geophysics 53(3):321–328. https://doi.org/10.1002/cjg2.1500
27. Langbein J (2008) Noise in GPS displacement measurements from Southern California and Southern Nevada. J Geophys Res 113:B05405. https://doi.org/10.1029/2007JB005247
28. Mémin A, Boy J, Santamaría-Gómez A (2020) Correcting GPS measurements for non-tidal loading. GPS Solutions: The Journal of Global Navigation Satellite Systems 24(2):2103–1113. https://doi.org/10.1007/s10291-020-0959-3
29. Menemenlis D, Campin J-M, Heimbach P et al (2008) ECCO2: High resolution global ocean and sea ice data synthesis. Mercat Ocean Q Newsl 31:13–21
30. Ray J, Altamimi Z, Collilieux X, van Dam T (2008) Anomalous harmonics in the spectra of GPS position estimates. GPS Solutions 12(1):55–64. https://doi.org/10.1007/s10291-007-0067-7

31. Rodell M, Houser PR, Jambor UE, A et al (2004) The Global Land Data Assimilation System. Bulletin of The American Meteorological Society 85(3):381–394
32. Reichle RH, Koster RD, Lannoy GD, Forman BA, Liu Q, Mahanama S et al (2011) Assessment and enhancement of merra land surface hydrology estimates. J Clim 24(24):6322–6338
33. Sun H, Ducarme B, Dehant V (1995) Effect of the atmospheric pressure on surface displacements. J Geodesy 70(3):131–139. https://doi.org/10.1007/BF00943688
34. van Dam T, Blewitt G, Heflin M (1994) Atmospheric pressure loading effects on Global Positioning System coordinate determinations. Journal of Geophysical Research Solid Earth 99(B12):23939–23950. https://doi.org/10.1029/94JB02122
35. van Dam T, Wahr J, Milly P, Shmakin A, Blewitt G, Lavallée D, Larson K (2001) Crustal displacements due to continental water loading. Geophys Res Lett 28(4):651–654. https://doi.org/10.1029/2000GL012120
36. van Dam T, Altamimi Z, Collilieux X, Ray J (2010) Topographically induced height errors in predicted atmospheric loading effects. J Geophys Res 115:B07415. https://doi.org/10.1029/2009JB006810
37. van Dam T, Collilieux X, Wuite J et al (2012) Nontidal ocean loading: amplitudes and potential effects in GPS height time series. J Geodesy 86(11):1043–1057. https://doi.org/10.1007/s00190-012-0564-5
38. Van Dam TM, Wanr J (1998) Modeling environment loading effects: a review. Phys Chem Earth 23(9):1077–1087. https://doi.org/10.1016/S0079-1946(98)00147-5
39. Williams SD, P, Bock Y, Fang P, Jamason P, Nikolaidis RM, Prawirodirdjo L, Miller M, Johnson DJ (2004) Error analysis of continuous GPS position time series. J Geophys Res 109:B03412. https://doi.org/10.1029/2003JB002741
40. Williams SD, P, Penna NT (2011) Non-tidal ocean loading effects on geodetic GPS heights. Geophys Res Lett 38: L09314. https://doi.org/ 10.1029/2011GL046940
41. Xu X, Dong D, Fang M et al (2017) Contributions of thermoelastic deformation to seasonal variations in GPS station position. GPS Solutions 21(3):1265–1274. https://doi.org/10.1007/s10291-017-0609-6
42. Yuan P, Li Z, Jiang W, Ma Y, Chen W, Sneeuw N (2018) Influences of Environmental Loading Corrections on the Nonlinear Variations and Velocity Uncertainties for the Reprocessed Global Positioning System Height Time Series of the Crustal Movement Observation Network of China. Remote Sensing 10(6):958. https://doi.org/10.3390/rs10060958
43. Yan H, Wu C, Zhu Y et al (2009) Contributions of thermal expansion of monuments and nearby bedrock to observed GPS height changes. Geophys Res Lett 36(13). https://doi.org/10.1029/2009GL038152
44. Zou R, Freymueller JT, Ding K et al (2014) Evaluating seasonal loading models and their impact on global and regional reference frame alignment. Journal of Geophysical Research Solid Earth 119(2):1337–1358. https://doi.org/10.1002/2013JB010186

Figures

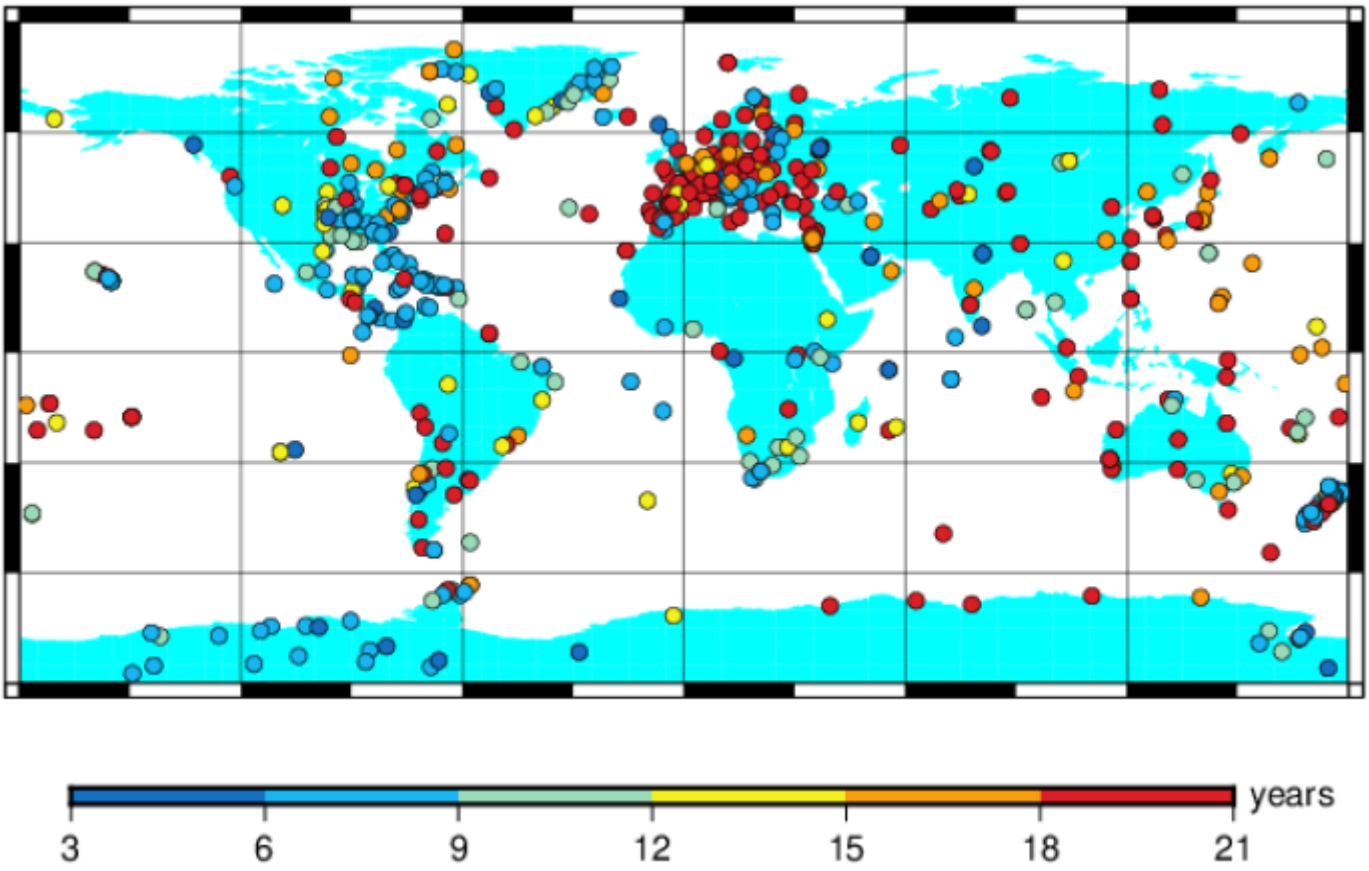

Figure 1

Distribution of global 631 GNSS stations

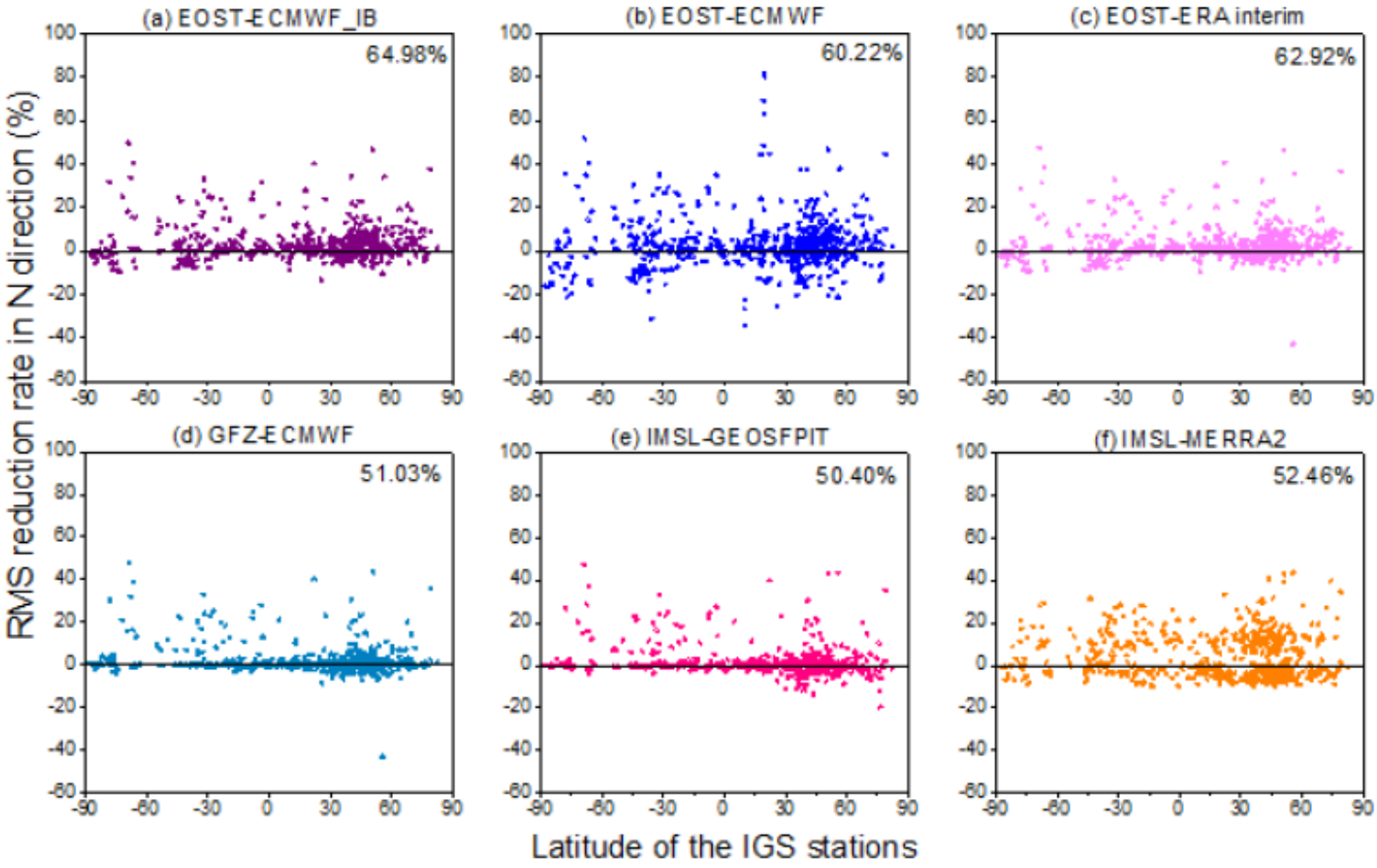

Figure 2

The distribution of the RMS reduction rate in N direction after ATML correction at different latitudes

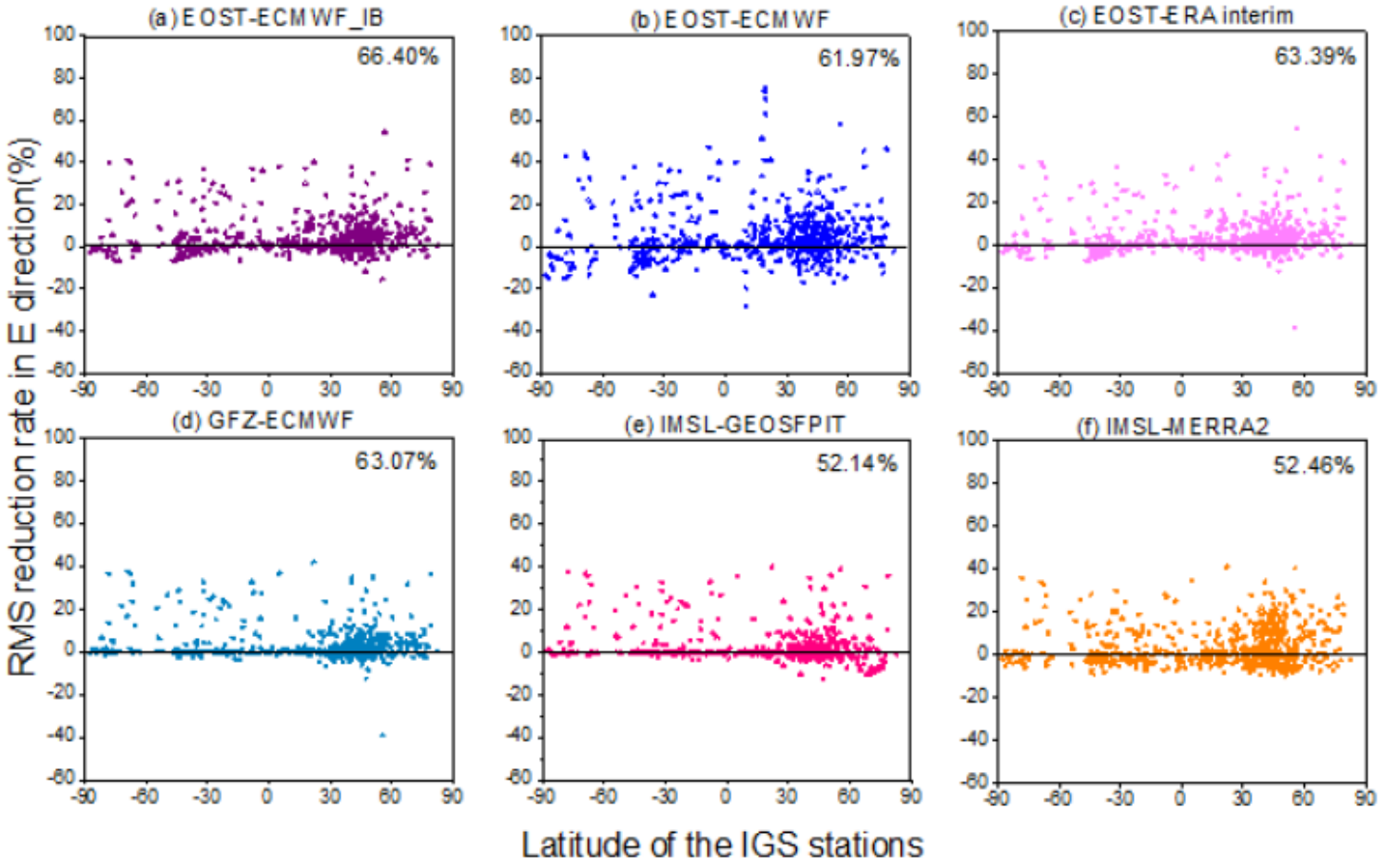

Figure 3

The distribution of the RMS reduction rate in E direction after ATML correction at different latitudes

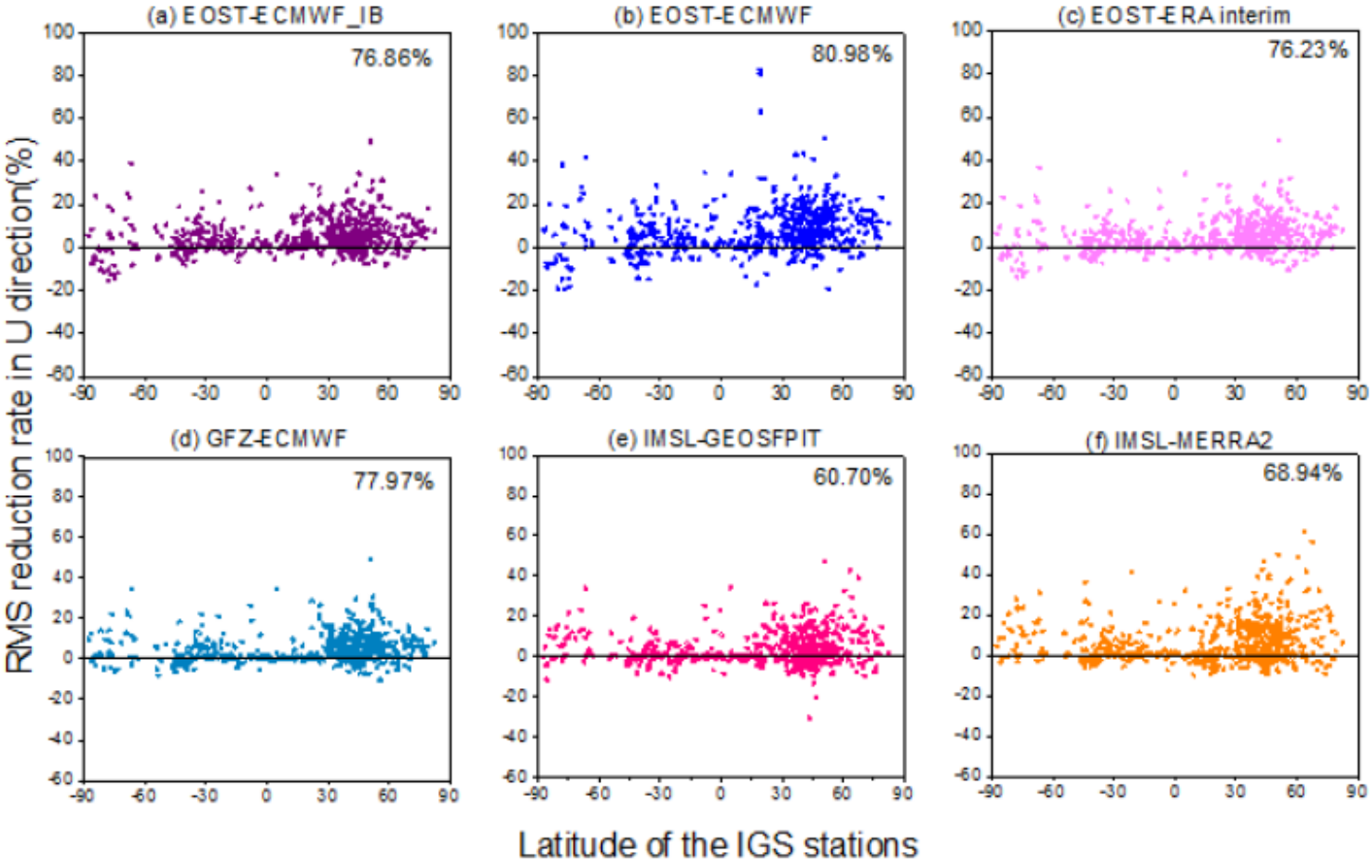

Figure 4

The distribution of the RMS reduction rate in U direction after ATML correction at different latitudes

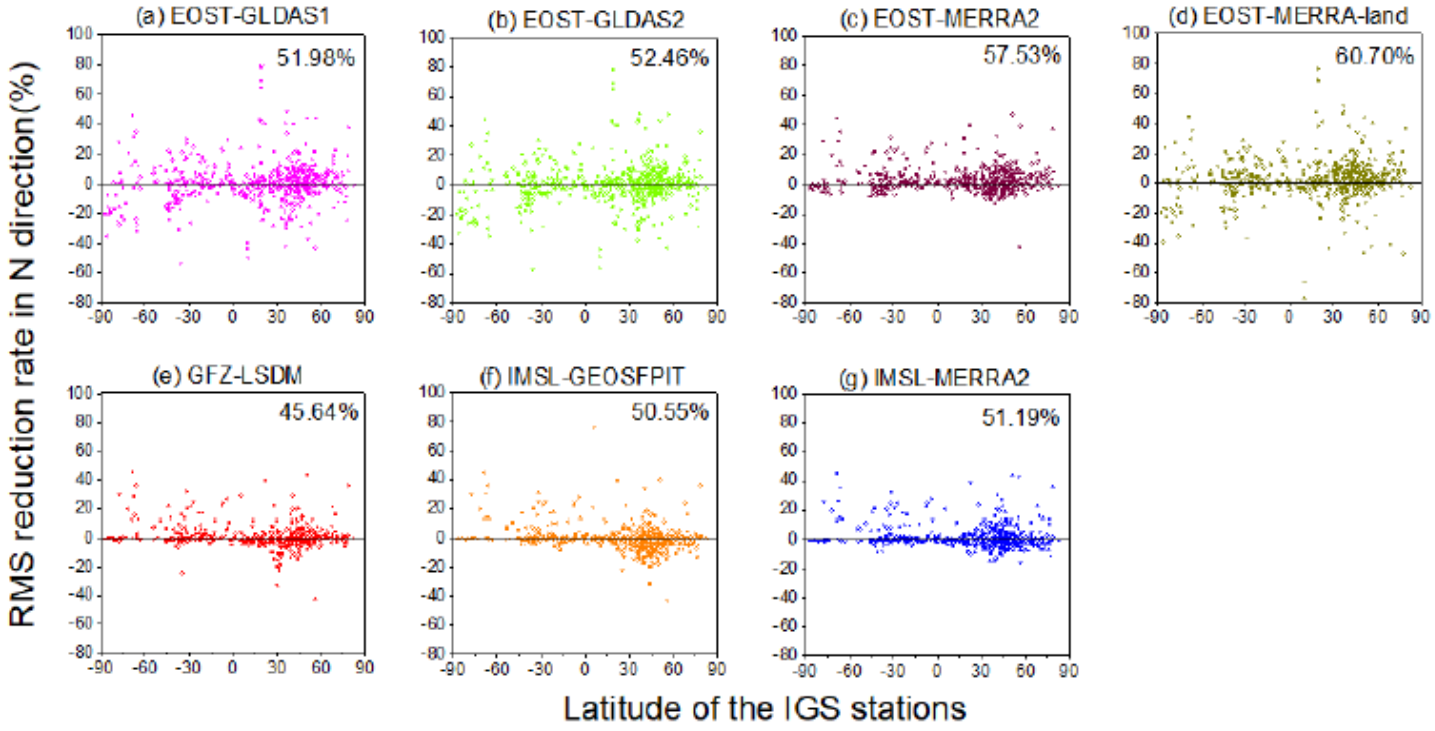

Figure 5

The distribution of the RMS reduction rate in N direction after HYDL correction at different latitudes

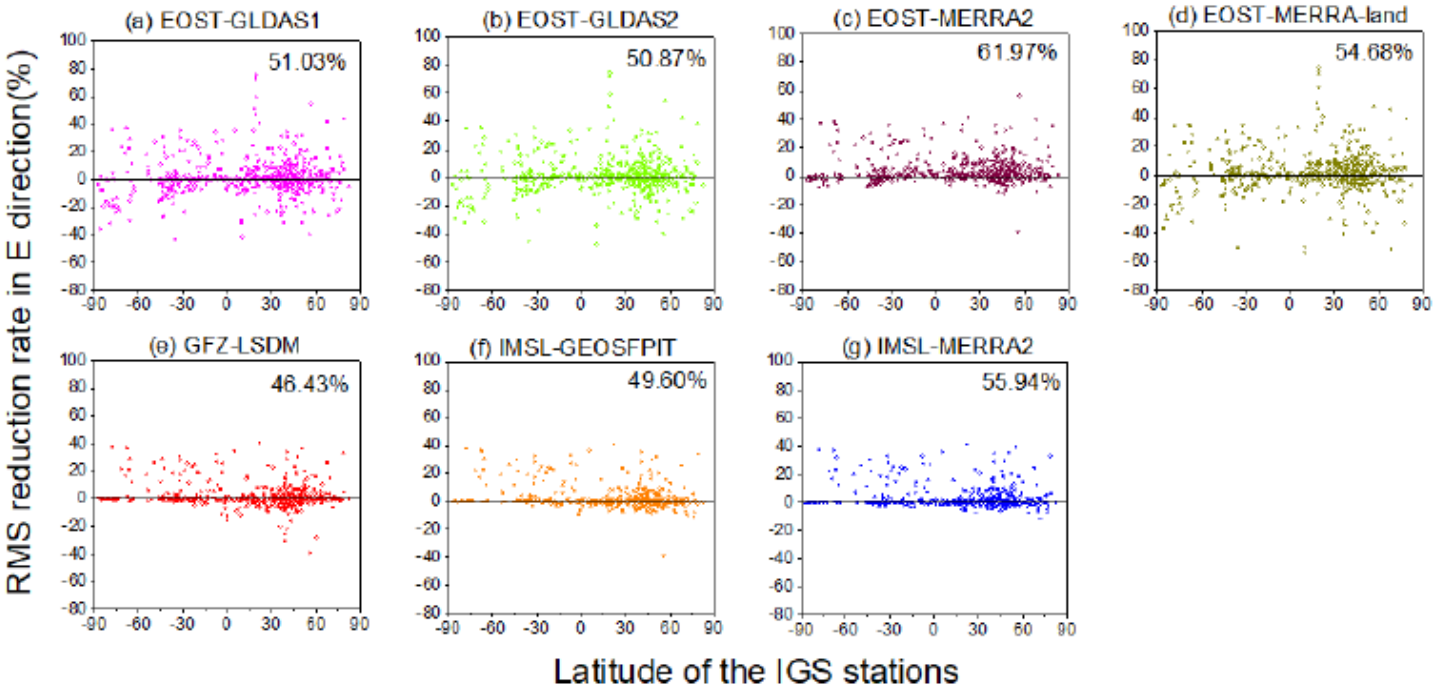

Figure 6

The distribution of the RMS reduction rate in E direction after HYDL correction at different latitudes

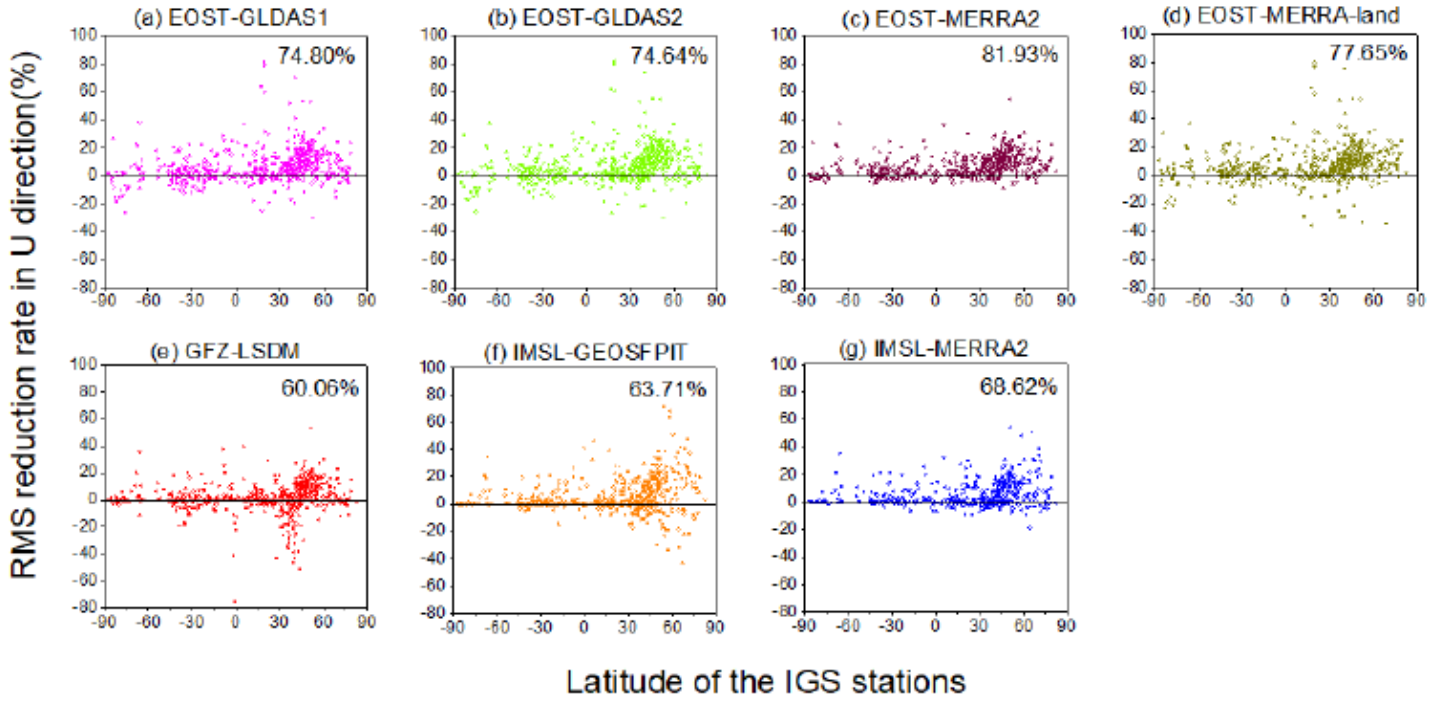

Figure 7

The distribution of the RMS reduction rate in U direction after HYDL correction at different latitudes

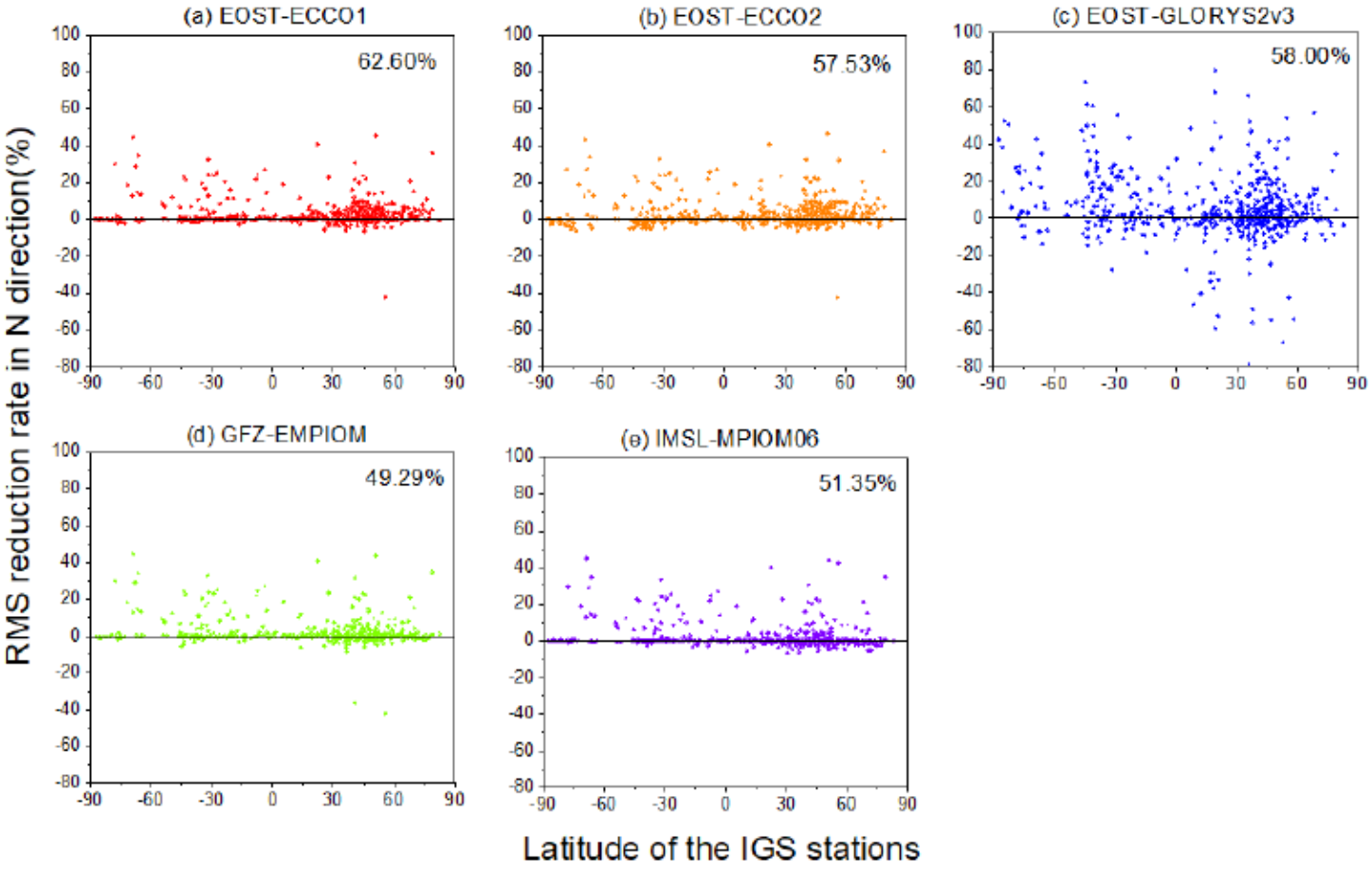

Figure 8

The distribution of the RMS reduction rate in N direction after NTOL correction at different latitudes

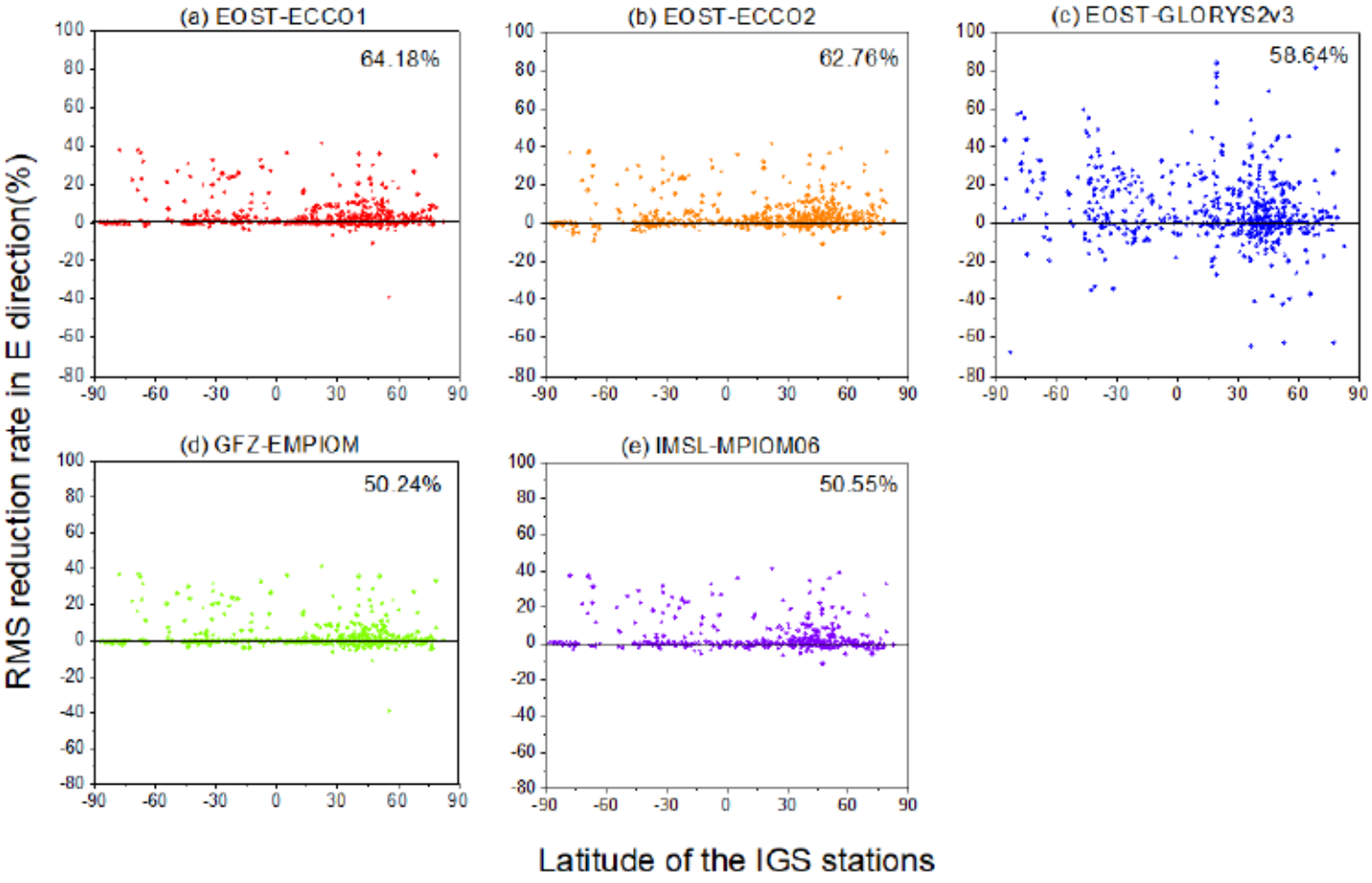

Figure 9

The distribution of the RMS reduction rate in E direction after NTOL correction at different latitudes

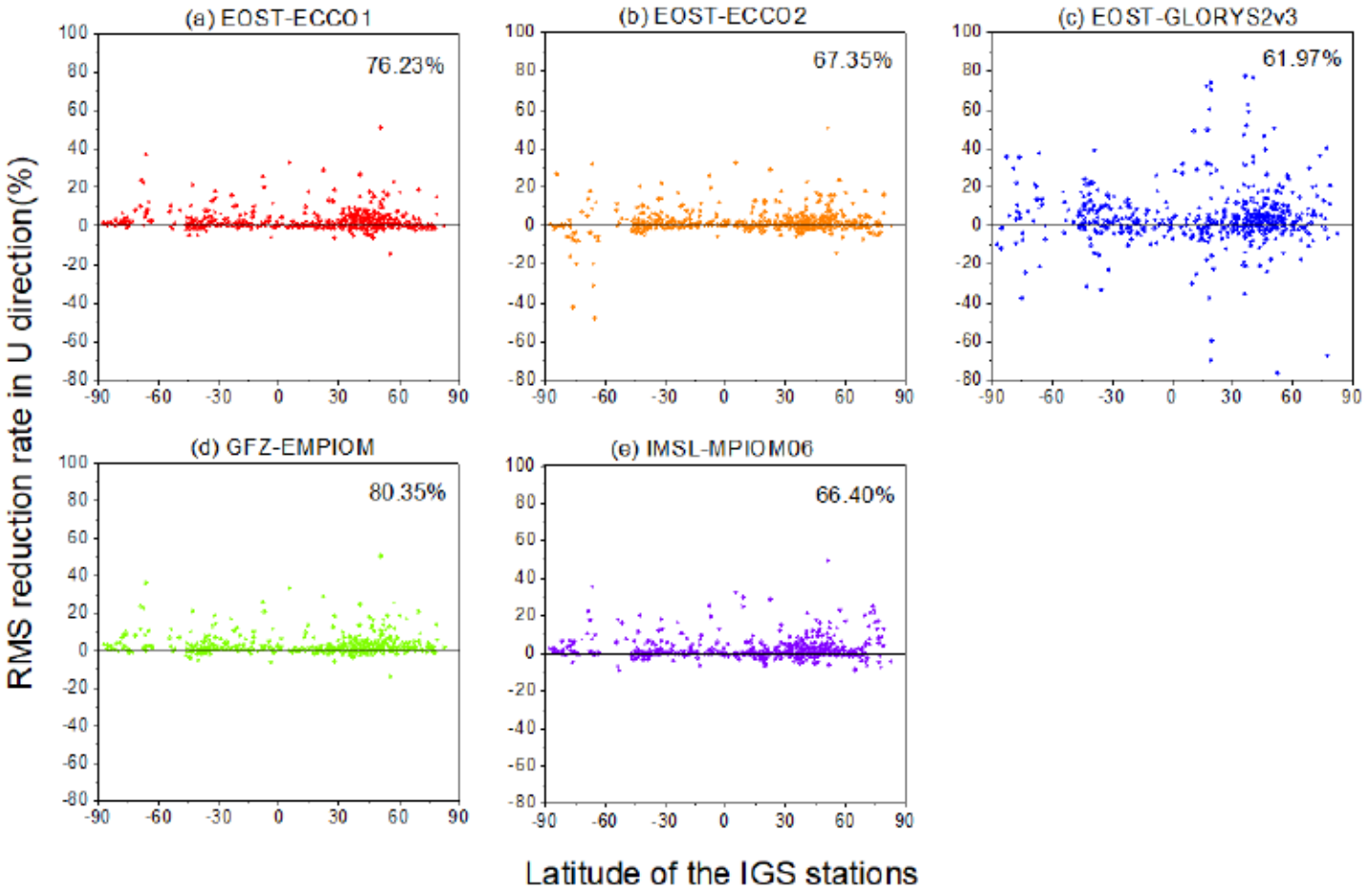

Figure 10

The distribution of the RMS reduction rate in U direction after NTOL correction at different latitudes

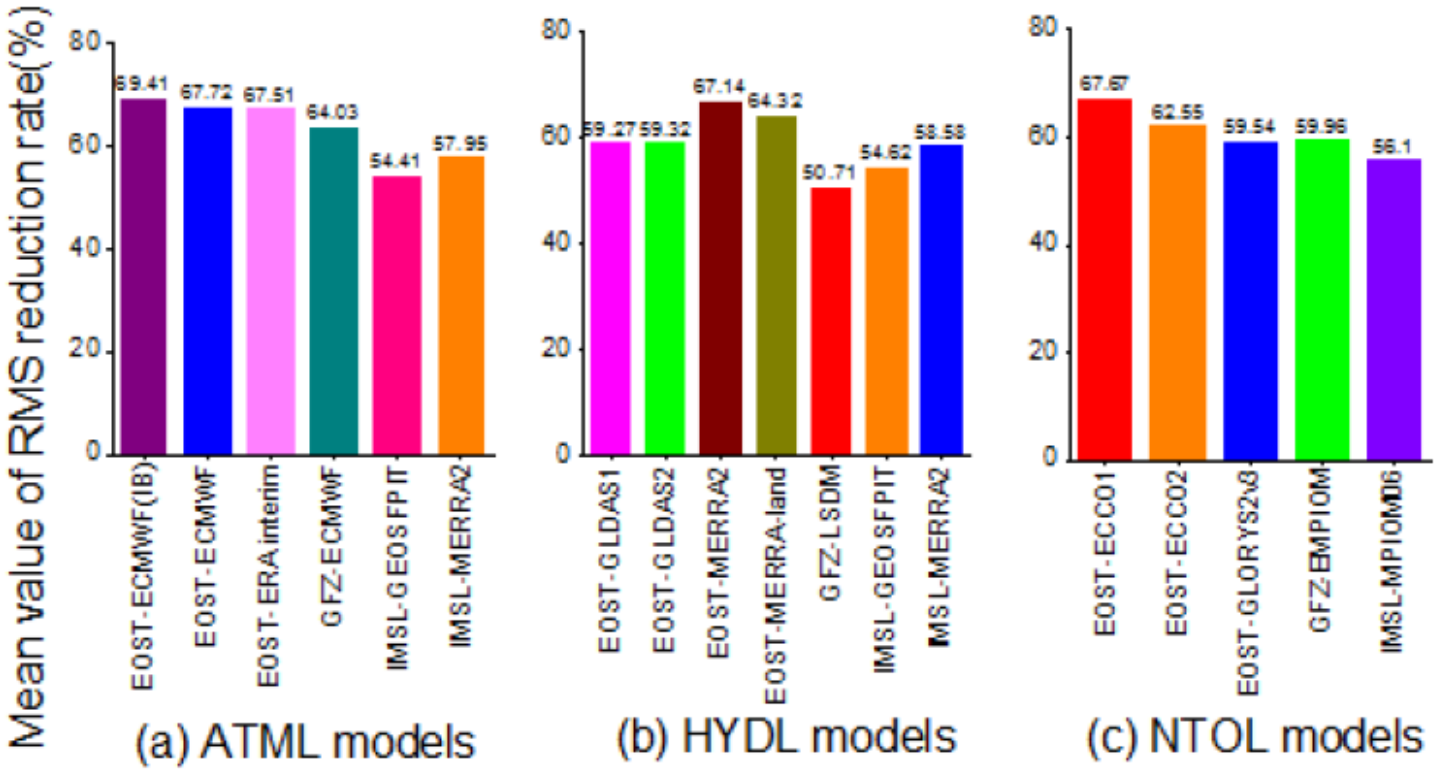

Figure 11

The average percentage of GNSS stations with positive RMS reduction rate after ELCs

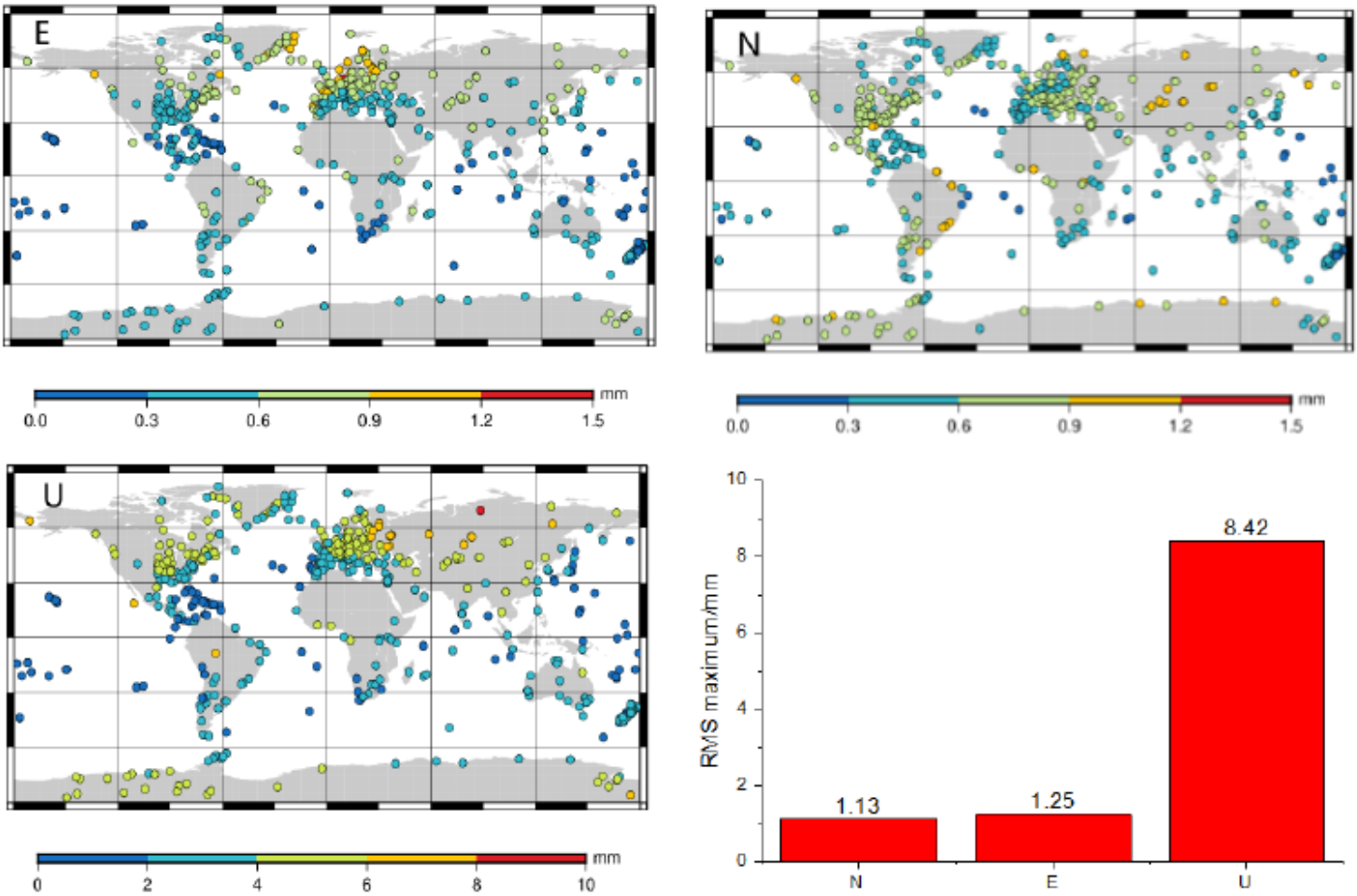

Figure 12

The RMS value and its maximum statistical distribution diagram of global IGS stations in E, N and U directions after the optimal ELCs

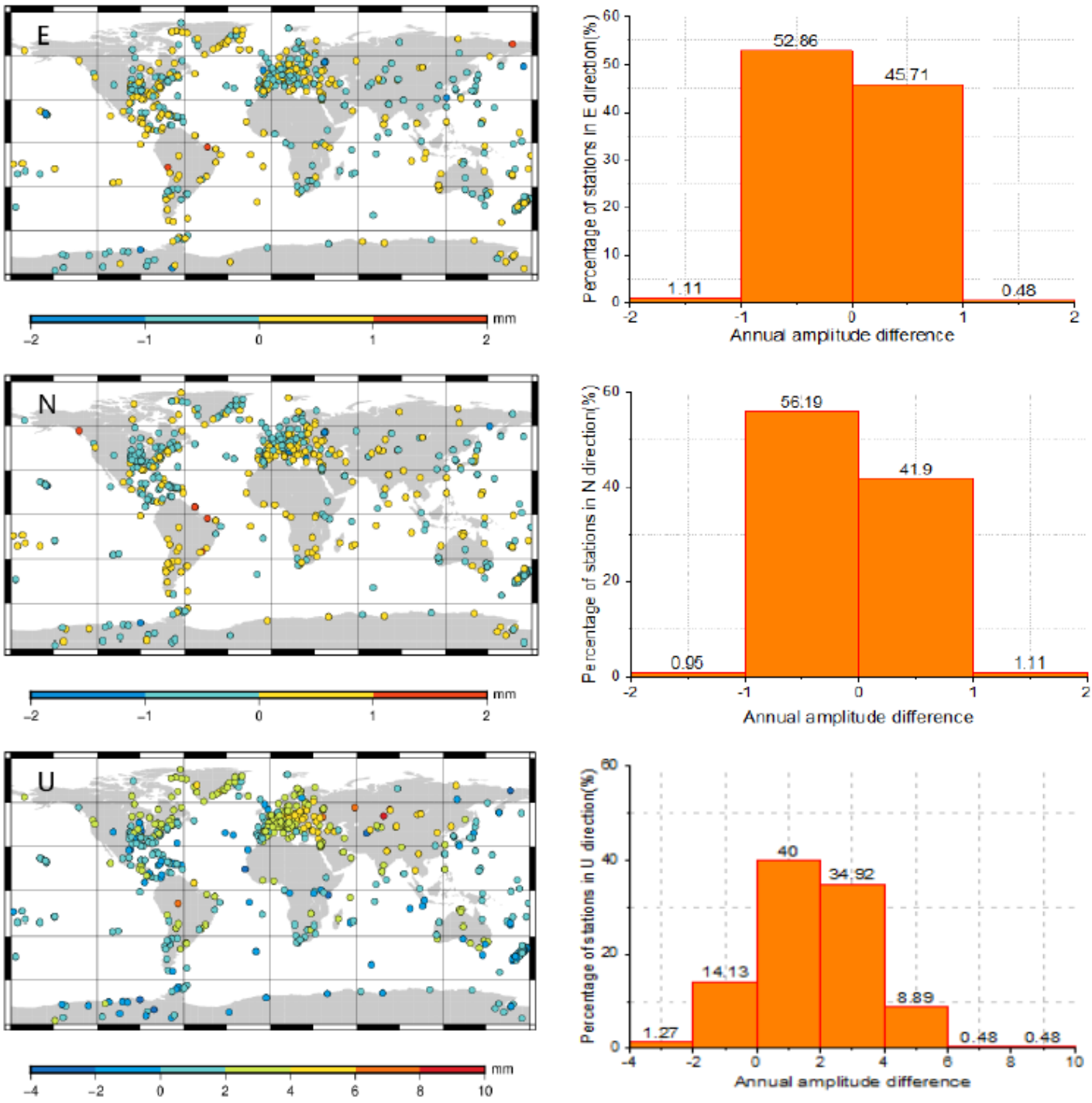

Figure 13

The distribution of annual amplitude difference and the percentage statistics of magnitude before and after ELCs in E, N and U directions

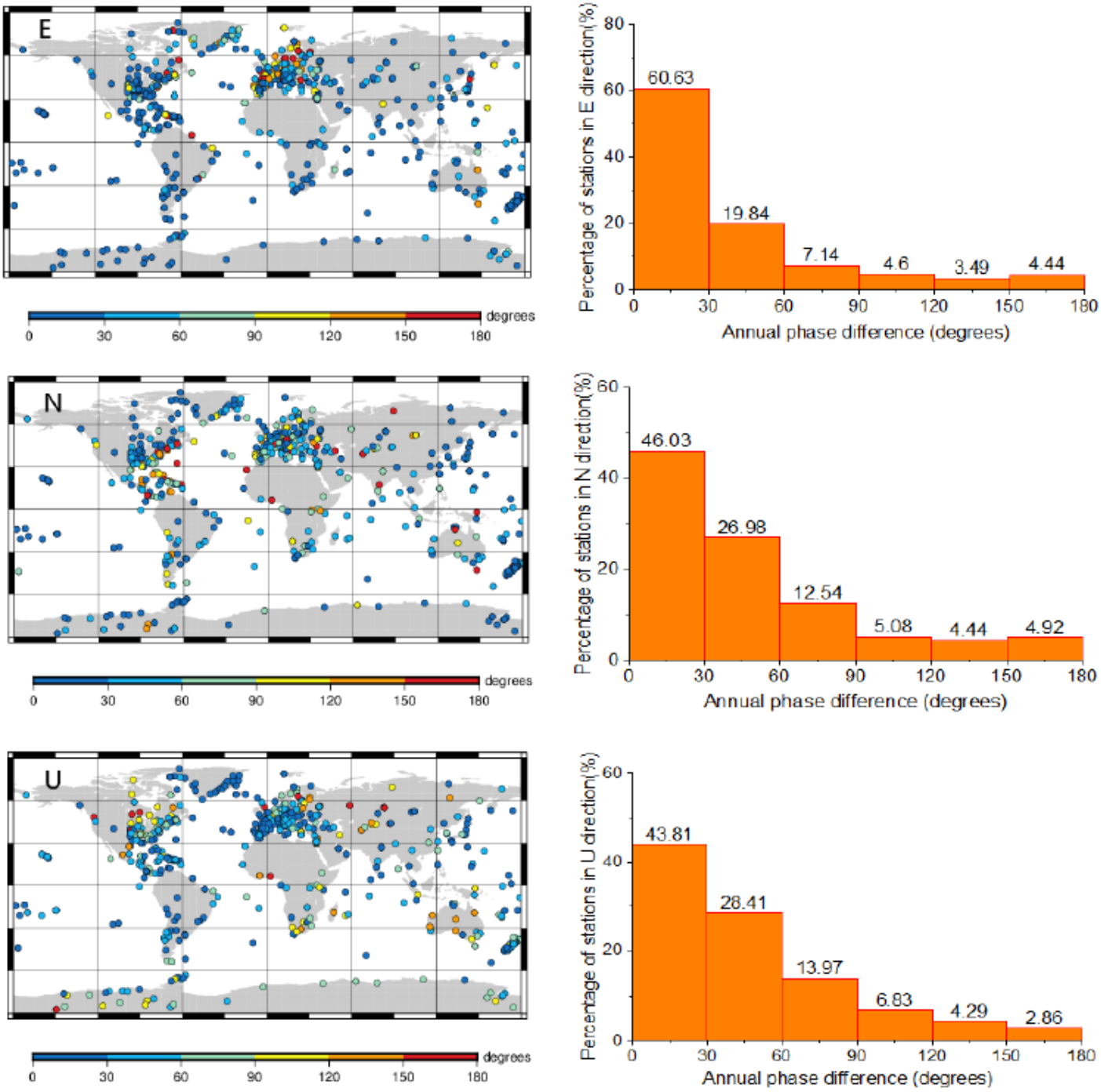

Figure 14

The distribution of absolute annual phase difference and the percentage statistics of magnitude before and after ELCs in E, N and U directions

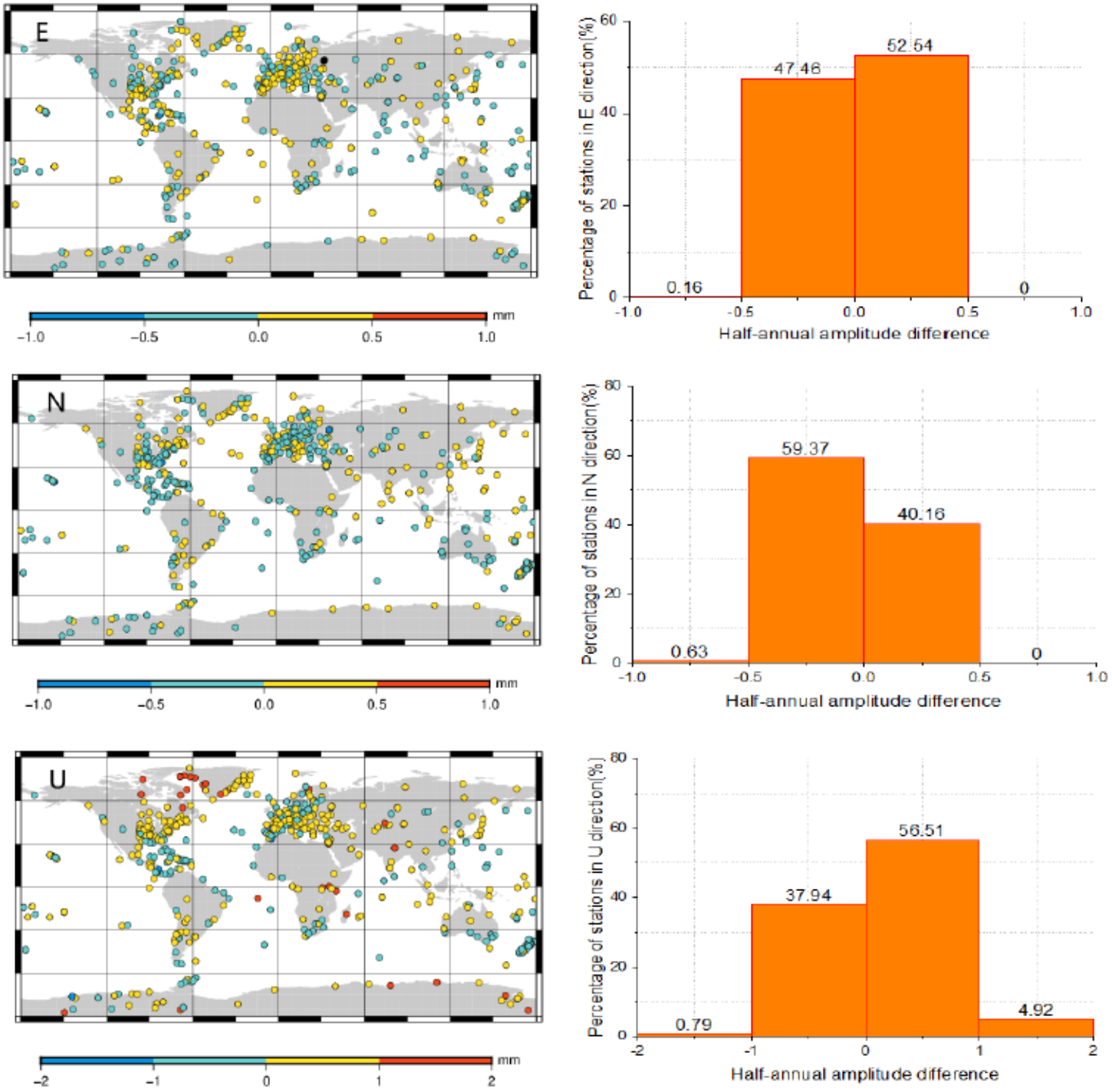

Figure 15

The distribution of half-annual amplitude difference and the percentage statistics of magnitude before and after ELCs in E, N and U directions

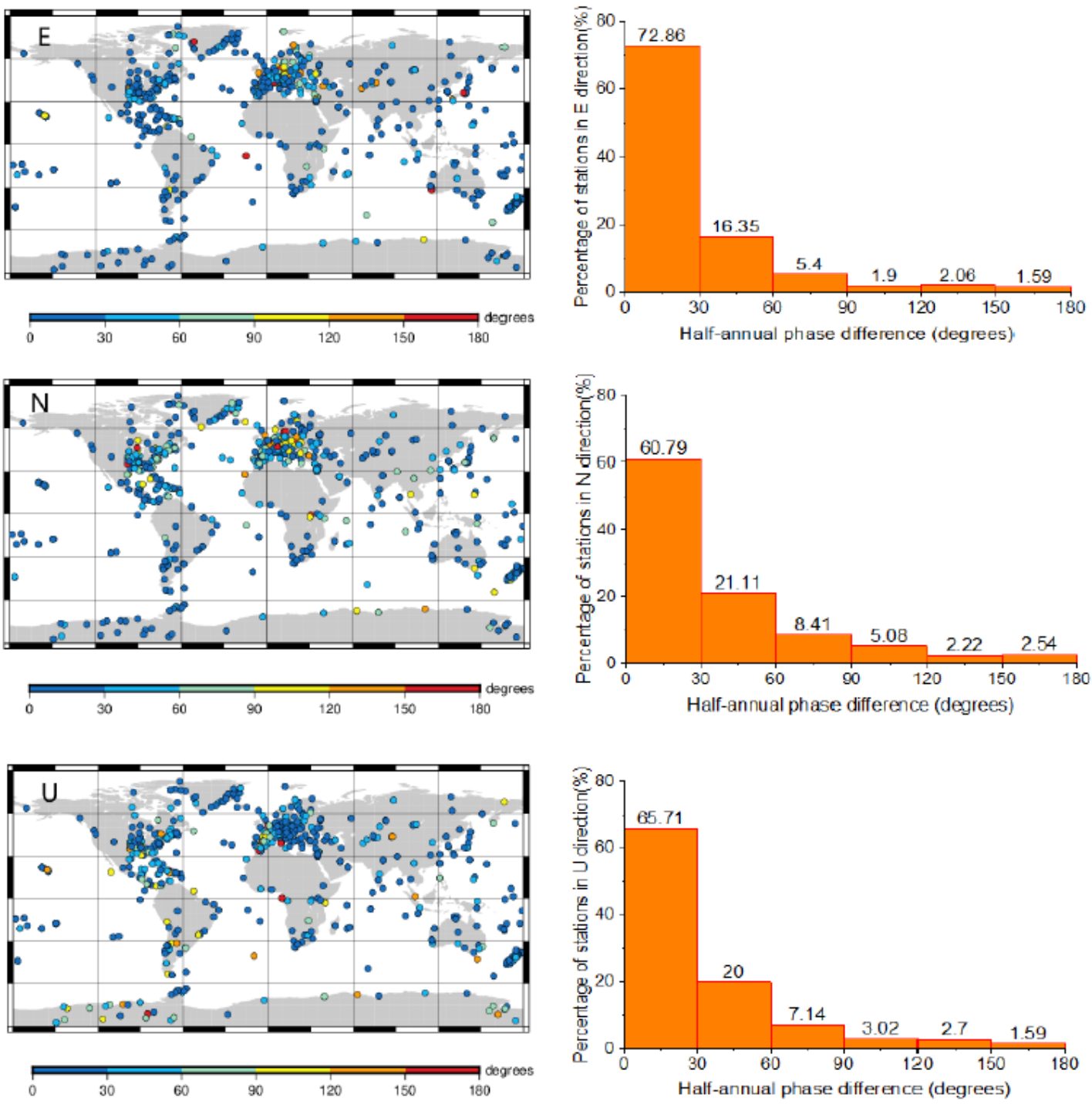

Figure 16

The distribution of the absolute half-annual phase difference and the percentage statistics of magnitude before and after ELCs in E, N and U directions

Supplementary Files

This is a list of supplementary files associated with this preprint. Click to download.

- Graphicalabstract.png